Applied Surface Science 605 (2022) 154569

Contents lists available at ScienceDirect

Applied Surface Science

journal homepage: www.elsevier.com/locate/apsusc

Short Communication

High uniformity and stability of graphene transparent conducting electrodes by dual-side doping

Min Ji Im [a,b], Seok-Ki Hyeong [a,c], Jae-Hyun Lee [c], Tae-Wook Kim [d], Seoung-Ki Lee [e], Gun Young Jung [b,*], Sukang Bae [a,*]

[a] Functional Composite Materials Research Center, Korea Institute of Science and Technology, Chudong-ro 92, Bongdong-eup, Wanju-gun, Jeonbuk 55324, Republic of Korea
[b] School of Materials Science and Engineering, Gwangju Institute of Science and Technology (GIST), 123 Cheomdan-gwagiro, Buk-gu, Gwangju 61005, Republic of Korea
[c] Department of Energy Systems Research and Department of Materials Science and Engineering, Ajou University, Suwon, Gyeonggi-do 16499, Republic of Korea
[d] Department of Flexible and Printable Electronics, Jeonbuk National University, Jeonbuk 54896, Republic of Korea
[e] School of Materials Science and Engineering, Pusan University, Busan 46241, Republic of Korea

ARTICLE INFO

Keywords:
Dual-side doping
p-doping
Nafion
Figure of Merit
Sheet resistance
Thermal stability
Chemical stability

ABSTRACT

Chemical doping is an efficient method to tailor the electrical properties of graphene transparent conductive electrodes. In general, chemically doped graphene by single-side exhibits a drawback of high conductivity but inferior uniformity and stability after exposure to chemical solvent or annealing process. Here, we report a highly uniform and stable graphene transparent conducting electrodes doped by dual-side with macro- and small molecular organic dopants such as Nafion on the top and benzimidazole (BI) at the bottom. The electrical properties, optical properties, and stability were compared depending on the top-side dopants. Dual-side doping showed a higher work function (>5 eV), and a uniform low sheet resistance (less than 200 Ω sq^{-1}) compared to the single-side doping. The Dual-N exhibited a relatively higher figure of merit (FoM, σ_{DC}/σ_{op} ~ 62.38), a smoother surface (R_{rms} ~ 0.54 nm), and a superior thermal/chemical stability than the Dual-A, showing the potential possibility as alternative electrodes for next-generation flexible electronic devices.

1. Introduction

Over the past several years, graphene has garnered considerable attention as an alternative transparent conductive electrode (TCE) to replace the commercial indium tin oxide (ITO) in flexible electronics owing to its high optical transparency, high electrical conductivity, chemical stability, and mechanical flexibility [1–3]. Chemical vapor deposition (CVD) is the most popular approach to grow a large-scale graphene film, which is single [4,5] or polycrystalline [6,7]. As synthesized graphene (PG, monolayer) has a high sheet resistance (R_{sh} > 500 Ω sq^{-1}) and a low work function (WF ~ 4.3 eV) compared with those of ITO (WF ~ 4.8 eV, R_{sh} ~ 10 Ω sq^{-1}) respectively [8,9], thereby doping of graphene has been performed to modulate them [10,11]. Chemical doping is a simple and effective way to enhance the electrical properties of graphene. Doping effect is made via dopant adsorption on the graphene surface, which is preferably occurred at the grain boundaries or defects [12,13]. Therefore, doping was more effective in polycrystalline graphene containing grain boundaries than the single-crystalline graphene.

Several dopant types are reported such as acid (HNO_3, HCl, H_2SO_4) [14–17], metal chloride ($RhCl_3$, $IrCl_3$, $MoCl_3$, $AuCl_3$, $SoCl_2$) [10,18–19], and polymer (PEDOT, TFSA, Nafion) [20–23]. Acid-doped graphene initially has a low R_{sh} under ambient conditions, but R_{sh} is significantly increased with time because of the volatility of acids [17]. After doping with metal chlorides, graphene has a low optical transmittance due to the metal cluster formation on the graphene surface, which could be a leakage path for electrical current [24]. In addition, the R_{sh} degrades under heat treatment [25,26]. Polymer-doped graphene has a relatively uniform surface roughness, but it has a comparatively lower doping effect [23,27,28]. The conventional single-side doping could not provide sufficient doping strength because the transferred charges are proportional to the graphene surface area in contact with the dopants [29]. Dual-side doping, in which dopants are positioned on both sides, has been explored, but there were still technical challenges. Xu et al. reported dual-side doped graphene with a poly(3-hexylthiophene-2,5-diyl) (P3HT) on the top and bis(trifluoromethanesulfonyl)-amide

* Corresponding authors.
E-mail addresses: gyjung@gist.ac.kr (G. Young Jung), sbae@kist.re.kr (S. Bae).

https://doi.org/10.1016/j.apsusc.2022.154569
Received 27 June 2022; Received in revised form 11 August 2022; Accepted 14 August 2022
Available online 24 August 2022

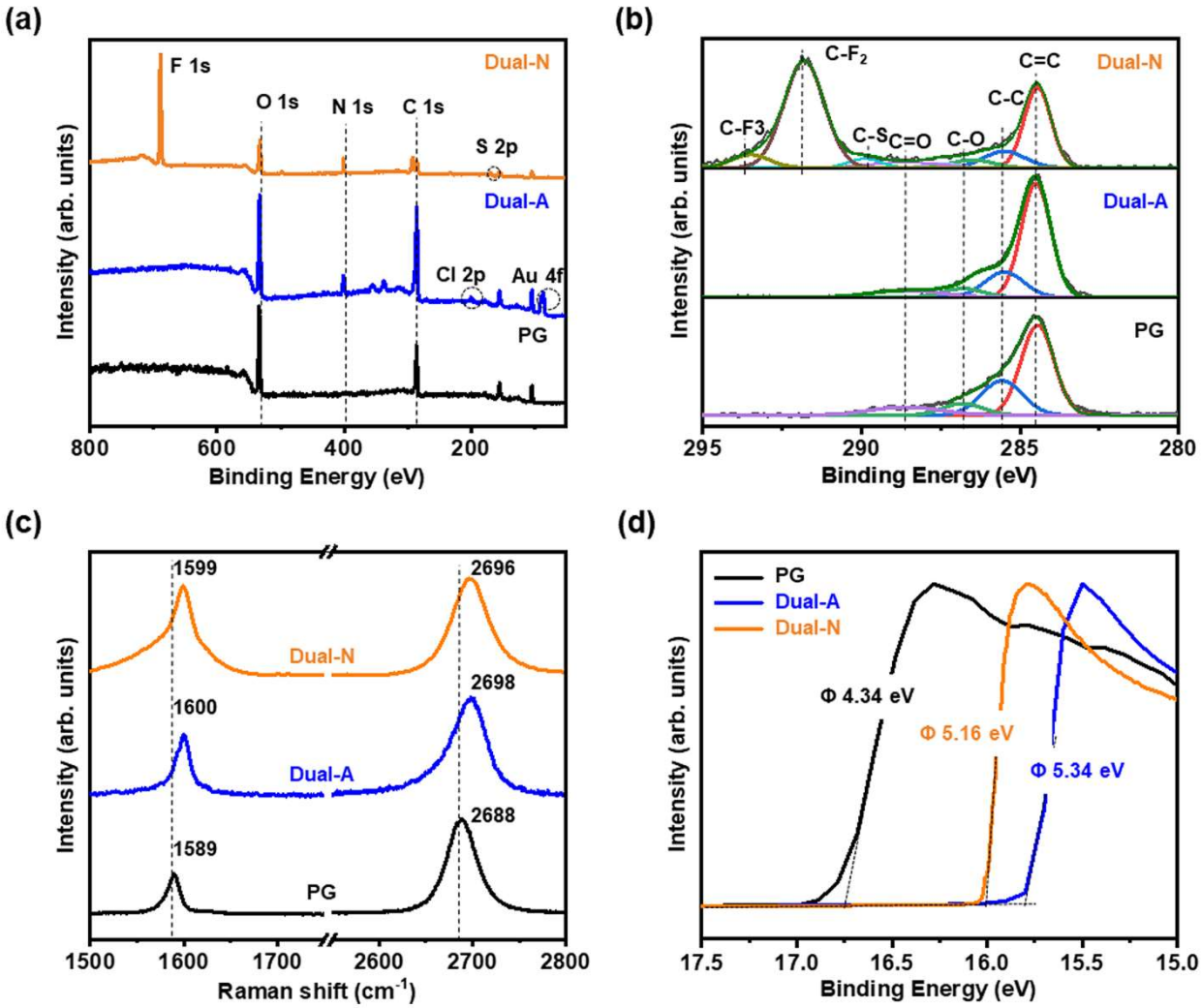

Fig. 1. (a) XPS survey spectra, (b) High-resolution C 1 s XPS spectra, (c) Raman spectra, and (d) UPS spectra of the PG, Dual-A, and Dual-N.

(TFSA) on the bottom [30]. However, the film should be exposed to sunlight (AM 1.5G) for at least 1 h to have the doping effect prior to photovoltaic application. Kim et al. reported dual-side doping with diethylenetriamine (DETA) on top and in contact with amine-functionalized self-assembled monolayers (SAMs) on a SiO_2/Si substrate [29]. In this case, the SAM-treatment should be done before the graphene transfer to the substrate.

In this study, we performed dual-side doping to strengthen the doping effect on both sides; bottom-side doping with Benzimidazole (BI) and top-side doping with $AuCl_3$ (Dual-A) or Nafion (Dual-N). Bottom doping was made spontaneously during the graphene transfer process without any substrate treatment and the doping effect was immediate. Dual-side doped graphene films are compared with PG and single-side doped graphene films. The dual-side doping with Nafion revealed the best properties in terms of electrical, optical properties, and stability as well, providing the potential use for the flexible electrodes.

2. Experimental section

2.1. Graphene synthesis and transfer

A monolayer of graphene was grown on a 25–μm–thick copper (Cu) foil by chemical vapor deposition. The Cu foil was loaded into the chamber and gradually heated upto 1000 °C under H_2 (100 sccm) atmosphere. The graphene was synthesized under a gas mixture of CH_4 (125 sccm) and H_2 (100 sccm) for 30 min at 1000 °C. The chamber was then cooled down to room temperature under H_2. After graphene growth, poly(methyl methacrylate) (PMMA, 46 mg mL^{-1} in chlorobenzene) was spin-coated onto the graphene-grown Cu foil. The PMMA-coated graphene was rinsed with deionized water 3–5 times and transferred to the SiO_2/Si substrate or glass. It was then annealed at 80 °C to improve the adhesion of graphene onto the substrate. The samples were soaked in an acetone solution at 70 °C for 30 min to eliminate the PMMA to have only graphene on the substrate. The graphene that was grown on the other side of the Cu-foil was removed using oxygen plasma (100 W, 12 S, 160 mTorr). Then, the underlying Cu foil was etched in a 0.175 M ammonium persulfate ($(NH_4)_2S_2O_8$, APS) solution.

2.2. Doping

Molecular structures of dopants are shown in **Fig. S1**. For the bottom-side doping process, 3 mM of BI dopant was added into the APS etching solution; it was done simultaneously while etching the Cu foil [31]. For the top-side doping process, $AuCl_3$ (A) was dissolved in nitromethane solvent at different concentrations of 10, 20, 30, 40, and 50 mM. Nafion (N) was dissolved in isopropyl alcohol at different concentrations of 10, 20, 30, 40, 50 and 60 mM. The doping solution was spin-coated (2500 rpm for 1 min) on the transferred graphene. These samples doped only at the top side surface of graphene are hereafter called as Top-A and Top-N, depending on the dopant. In this time, the BI dopant was not added to the APS etching solution during the Cu foil etching. For the dual-side doped samples (Dual-A and Dual-N), the

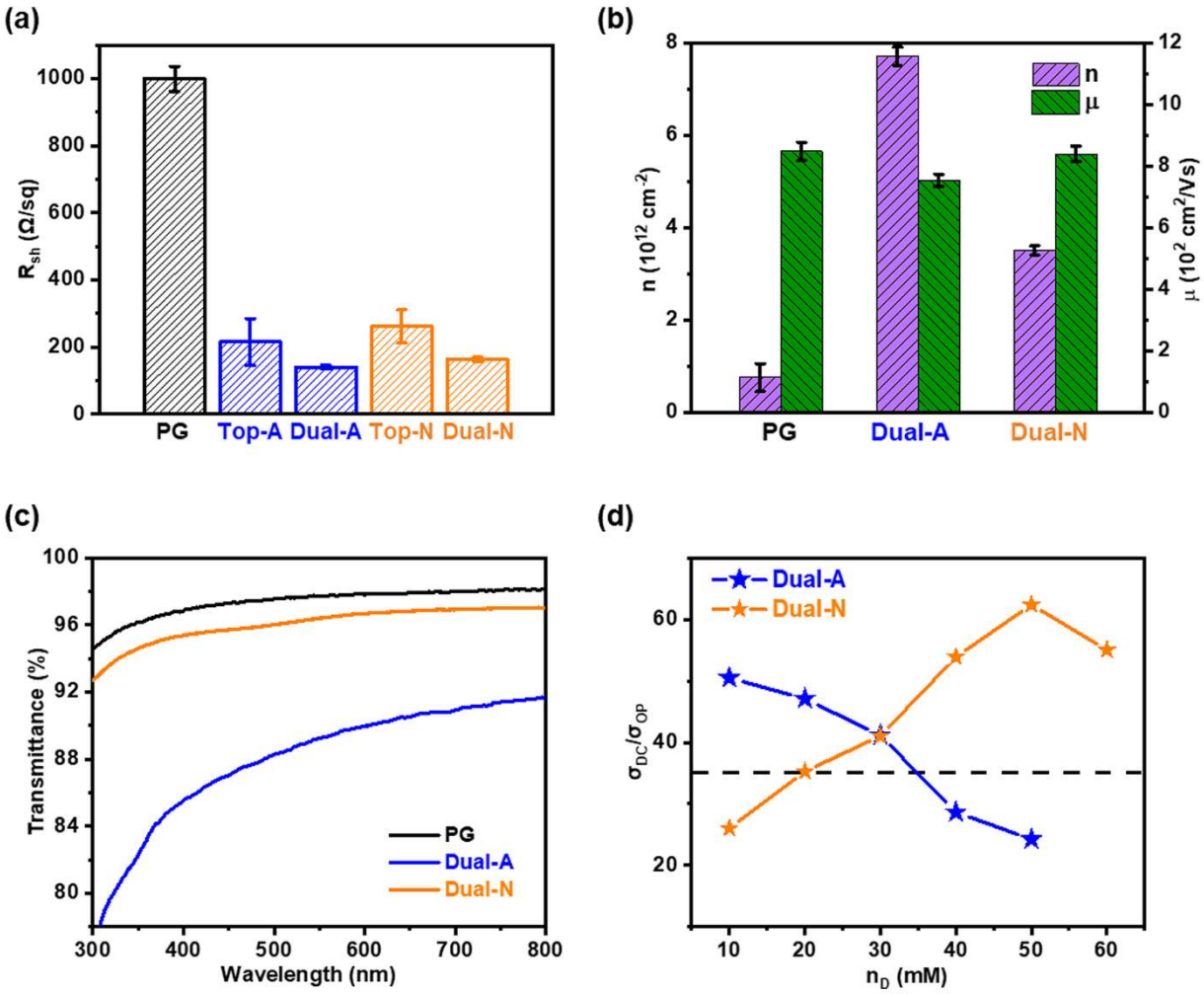

Fig. 2. Comparison of the (a) R_{sh}, (b) n and μ, and (c) transmittance of PG, Dual-A doped with $AuCl_3$ (50 mM), and Dual-N doped with Nafion (50 mM). (d) Figure of merit (σ_{DC}/σ_{OP}) with increasing the concentration of top-side dopant (n_D). Inner dotted line represents the minimum industry standards for TCEs.

doping solution was spin-coated on the transferred graphene which is already BI-doped on its bottom surface. The graphene doped with BI at only bottom side is hereafter called as Bottom-BI.

2.3. Characterization

To characterize the graphene doping state, Raman spectroscopy (Horiba) analysis was performed using a 514 nm laser. The transmittance of graphene was characterized using an ultraviolet – visible (UV–Vis) spectrophotometer (Jasco, V-670). XPS (Thermo Scientific) analysis was performed using monochromatic Al Kα X-ray photons (hv = 1486.6 eV). The work function of graphene was measured using ultraviolet photoelectron spectroscopy (UPS) with He I radiation (21.2 eV). R_s was measured using a four-point probe (Dasol ENG).

3. Results and discussion

3.1. Characterization of dual-side doped graphene films

XPS was conducted to characterize the chemical bonding states of PG, Dual-A, and Dual-N. Both Dual-A and Dual-N exhibit a N 1 s peak at ~ 400.27 eV indicating that the adsorption of BI molecules (Fig. 1**(a)**). In addition, the Dual-A has Au^{3+} peaks (~87 eV, ~91 eV), Au^0 peaks (~84 eV, ~88 eV), and Cl 2p peaks (~198 eV, ~200 eV) (**Fig. S2(a – b)**). The Dual-N has a F 1 s peak (~689 eV) and a S 2p peak (~169 eV) (**Fig. S2(c – d)**). These results demonstrated that graphene was successfully doped on both sides. The SEM-EDS mappings of dual-side doped graphene films were included in **Fig. S3**, showing well-distributed dopant atoms. The XPS C 1 s spectra are deconvoluted in Fig. 1**(b)** to analyze the chemical bonding states before and after dual-side doping. The C 1 s spectra of PG and Dual-A consist of four peaks: C–C sp^2 bonding at 284.5 eV, C–C sp^3 bonding at 285.5 eV, C – O (hydroxyl) bonding at 286.8 eV, and C = O (carboxyl) bonding at 288.6 eV. The C 1 s spectra of Dual-N reveals not only graphene-related peaks (i.e., C–C sp^2 bonding (~284.5 eV), C–C sp^3 bonding (~285.5 eV)) but also Nafion-related chemical bonds (i.e., C–S (~289.9 eV), –CF (~287.5 eV), $–CF_2$ (~291.8 eV), and $–CF_3$ (~293.5 eV)). After Dual-A and Dual-N doping, the position of C–C sp^2 and C–C sp^3 bonding was not shifted, confirming no additional structure defects. The binding energy, peak intensity ratio, and FWHM of C 1 s spectra are summarized in **Table S1**. **Fig. S4** shows that the intensity ratio ($I_{C=C}/I_{C-C}$) increases from 2.6 (PG) to 4.48 (Dual-A), 4.8 (Dual-N), demonstrating that graphene was *p*-doped [10].

Raman spectroscopy was used to investigate the degree of doping (Fig. 1**(c)**). Compared with the G peak (~1589 cm^{-1}) of PG, the G peaks of Dual-A and Dual-N are blue shifted by 11 cm^{-1} and 10 cm^{-1}, respectively. The G peaks of only top side-doped Top-A and Top-N are blue-shifted by 6 cm^{-1} and 3 cm^{-1}, respectively (**Fig. S5**). The larger blue-shift of G peak indicates the stronger *p*-doping [32–34]. The intensity ratio (I_{2D}/I_G) of PG is 2.5, which is similar to the previously reported results [35,36]. The I_{2D}/I_G ratio of dual-side doping (1.5 for Dual-A and 1.2 for Dual-N) is lower than those of single-side doping (1.7 for

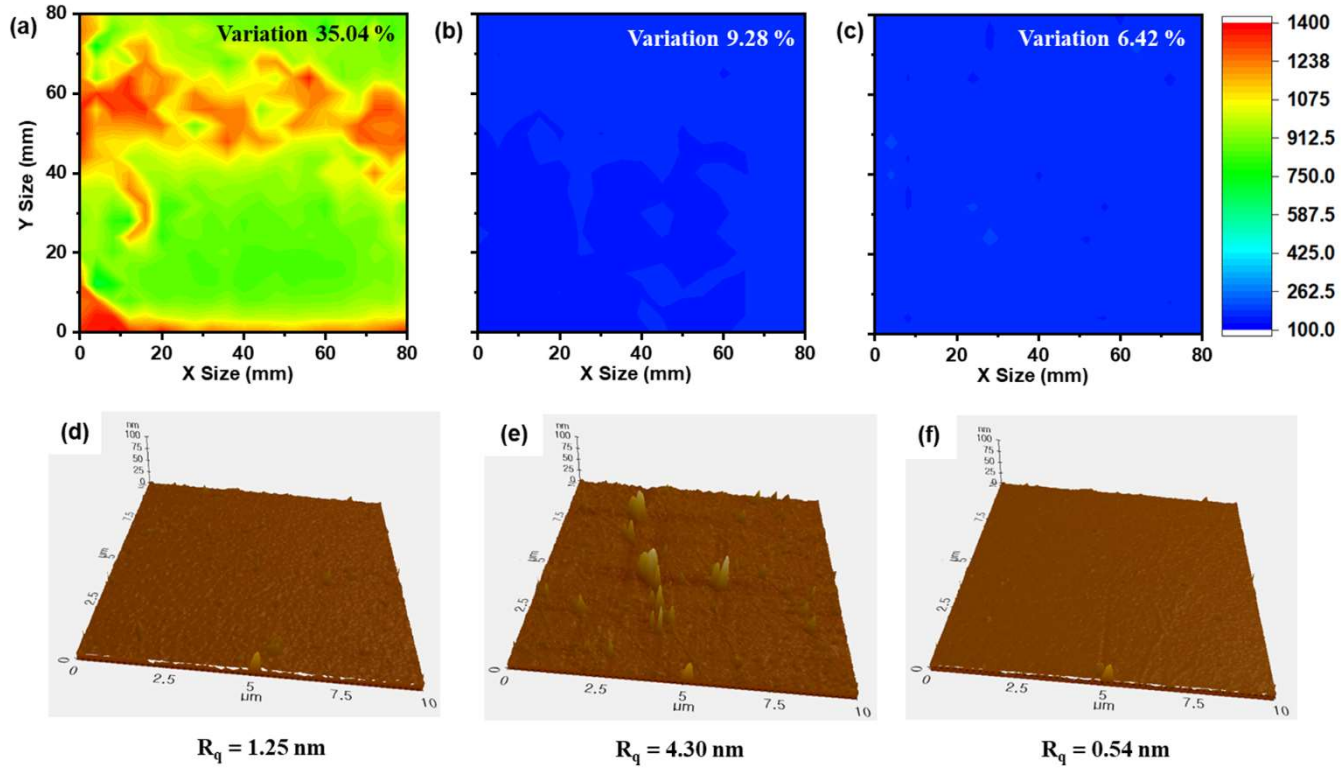

Fig. 3. R_{sh} mapping of the (a) PG, (b) Dual-A, and (c) Dual-N. AFM image of the (d) PG, (e) Dual-A, and (f) Dual-N.

Top-A and 1.5 for Top-N); the lower ratio (I_{2D}/I_G) implies that graphene was more *p*-doped [37,38]. Raman spectra show that the dual-side doping induced a stronger *p*-doping state than the single-side doping.

Ultraviolet photoelectron spectra (UPS) (Fig. 1**(d)**) were measured using a He I source (21.2 eV) to determine the WF of dual-side doped graphene film with the following equation:

$$WF = h\nu - (E_{cut-off} - E_f) \quad (1)$$

where, $h\nu$ and E_f are the excitation energy (He I source = 21.2 eV) and Fermi level edge (0 eV), respectively. The value of $E_{cut\text{-}off}$ can be measured from the intercept at the binding energy (x-axis) by linear extrapolation. The UPS spectra of Top-A and Top-N are presented in **Fig. S6**. Compared to PG, the top-side doping increased WF by 0.3–0.5 eV (4.64 eV for Top-N and 4.78 eV for Top-A) and the dual-side doping increased WF by 0.82–1 eV (5.16 eV for Dual-N and 5.34 eV for Dual-A), shifting the Fermi energy lower below the Dirac point. These results represent that the dual-side doping induced more *p*-doped graphene.

3.2. Electrical and optical properties of dual-side doped graphene films

The sheet resistance (R_{sh}) in Fig. 2**(a)** decreased from 1000 ± 37 Ω sq^{-1} (PG) to 214 ± 70 Ω sq^{-1} and 261 ± 50 Ω sq^{-1} for the Top-A doped with $AuCl_3$ (50 mM) and Top-N doped with Nafion (50 mM), respectively. Obviously, the Dual-A doped with $AuCl_3$ (50 mM) and Dual-N with Nafion (50 mM) exhibit lower R_{sh} values (Dual-A: 139.91 ± 6.24 Ω sq^{-1}, Dual-N: 163.31 ± 5.5 Ω sq^{-1}).

The reason for the low sheet resistance was investigated through Hall effect measurements **(**Fig. 2**(b))**. The carrier density of PG was found to be 7.62 × 10^{12} cm^{-2}, which is similar to the previously reported values [39]. After dual-side doping with 50 mM top-side dopants, the carrier density increased to 7.71 × 10^{13} cm^{-2} for Dual-A and 3.51 × 10^{13} cm^{-2} for Dual-N. The carrier motilities (μ) can be obtained by using the following equation:

$$\mu = \frac{\sigma V_H d}{IB}$$

where σ, V_H, I, B, and *d* are the conductivity, applied Hall voltage, current, applied magnetic field (0.560 T) and graphene thickness, respectively. The calculated mobility of PG is 848 cm^2 V^{-1} s^{-1}, which is similar to previous result [39]. Interestingly, the Dual-A showed a lower mobility (750 cm^2 V^{-1} s^{-1}) because the $AuCl_3$ dopant acted as impurities. In comparison, the calculated carrier mobility of Dual-N (840 cm^2 V^{-1} s^{-1}) is similar to PG. Therefore, it was anticipated that the reduction of R_{sh} was mainly due to the increase of carrier density.

Fig. 2**(c)** shows the optical transmittance spectra of PG, Dual-A, and Dual-N in 300–800 nm wavelength range. The transmittance is 97.7 % at 550 nm for PG. After dual-side doping with 50 mM top-side dopants, the transmittance of Dual-A (89.75 %) is lower than that of Dual-N (96.40 %) because the gold nanoparticles generated by metal ion reduction on the graphene surface could scatter the incident light.

FoM (σ_{DC}/σ_{op}) of the doped graphene film was calculated from the measured optical and electrical properties to evaluate the performance of TCE. A higher FoM (σ_{DC}/σ_{op}) is indicative of better performance as TCE [22,39,40]. Fig. 2**(d)** presents a plot of the FoM (σ_{DC}/σ_{op}) with increasing the concentration of top-side dopant. This value can be calculated using the following equation:

$$T = \{1 + (\frac{Z_O}{2R_{sh}})(\frac{\sigma_{op}}{\sigma_{DC}})\}^{-2}$$

where, Z_O (377 Ω) represents the impedance of free space, R_{sh} is the sheet resistance, and T is the transmittance at 550 nm. The transmittance, R_{sh}, and FoM for the top-side doping and dual-side doping are shown in **Table S2** and **Table S3**, respectively, at different concentrations of top-side dopant.

The FoM value of Dual-A has the highest value of 50.49 at 10 mM $AuCl_3$ and then decreases with increasing concentration because the transmittance of Dual-A decreases by 6 % from 95.45 % (10 mM) to 89.75 % (50 mM) while the R_{sh} is reduced by 11.7 % from 158.47 Ω sq^{-1} (10 mM) to 139.91 Ω sq^{-1} (50 mM). The FoM value of Dual-N (62.38) increases with the dopant concentration of Nafion and is optimized at 50 mM; the transmittance of Dual-N slightly decreases by 0.6 % from

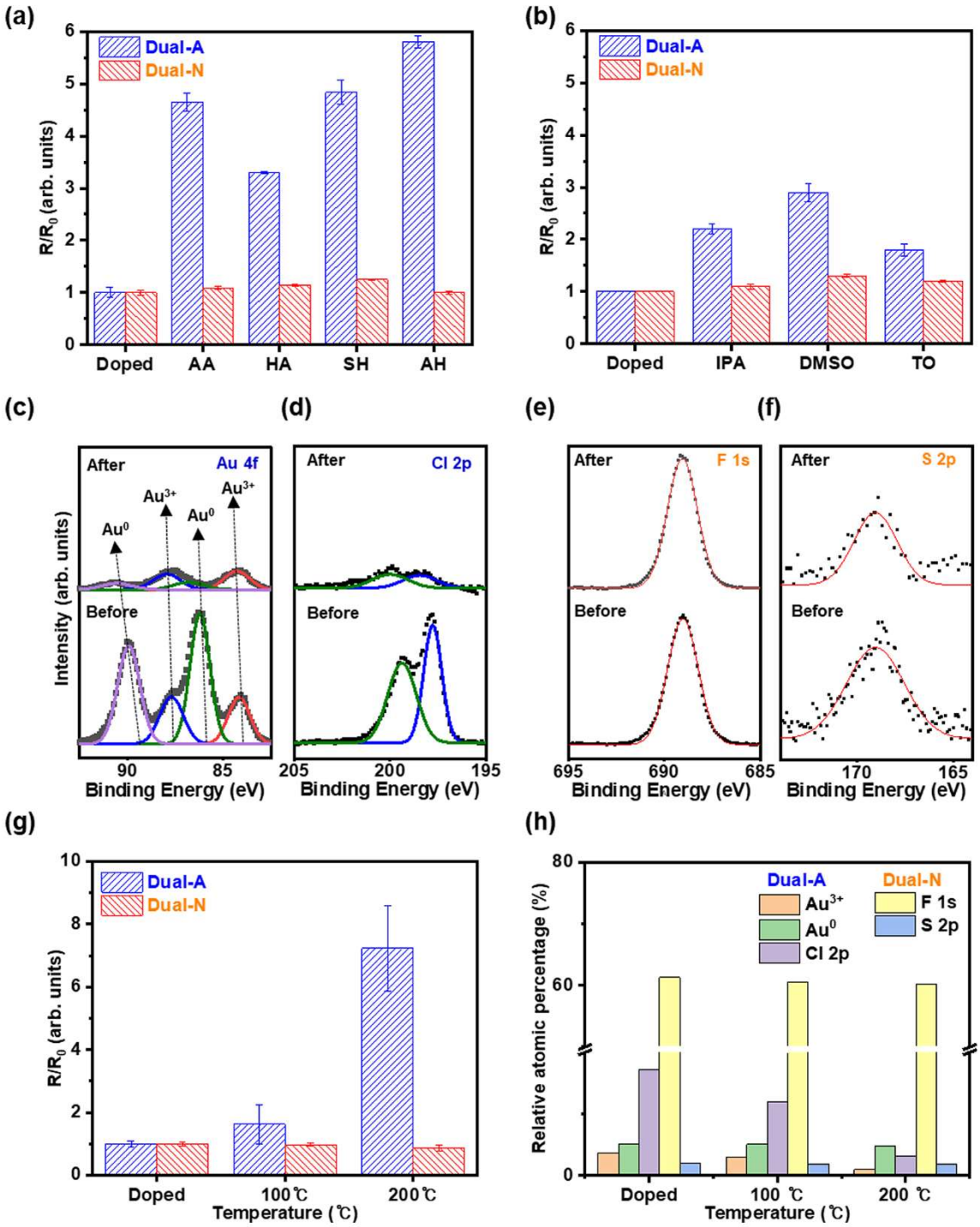

Fig. 4. Chemical and thermal stability. R_{sh} change under (a) various acid/base treatments (AA: acetic acid; HA: hydrochloric acid; AH: ammonium hydroxide; SH: sodium hydroxide), and (b) various solvent treatments (IPA: isopropyl alcohol, DMSO: dimethyl sulfoxide; TO: toluene), XPS change of the (c) Au 4f, (d) Cl 2p, (e) F 1 s, and (f) S 2p peak before and after AA treatment. (g) R_{sh} change and (h) relative atomic percent change at different annealing temperatures.

96.48 % (10 mM) to 95.90 % (60 mM) while the R_{sh} is much reduced by 59.6 % from 400.73 Ω sq^{-1} (10 mM) to 161.91 Ω sq^{-1} (60 mM). The FoM values of one-side doping reported in previous literatures [10,19–20,41] are compared in **Fig. S7**. The Dual-N has the highest FoM value (62.38) among the list, which exceeds industry requirements by far ($\sigma_{DC}/\sigma_{op} \sim 35$) [40].

3.3. R_{sh} uniformity of dual-side doped graphene films

To judge doping uniformity, R_{sh} mapping of PG, Dual-A, and Dual-N at an area of approximately 80 × 80 mm^2 was carried out (**Fig. 3 (a-c)**), and its variation was calculated with the following equation:

$$\text{Variation } (\%) = \left[\frac{(\text{Max.}R_{sh}\text{-Min.}R_{sh})}{2(\text{Ave.}R_{sh})}\right] \times 100$$

where, Max. R_{sh} is the highest R_{sh}, Min. R_{sh} is the lowest R_{sh}, and Ave. R_{sh} is the average R_{sh}. The higher variation means that the graphene is not uniformly doped. The variation for PG is 35.04 %, which is relatively high due to the PMMA residues. As shown in **Fig. S8**, the variation is 33.29 %, 25.96 %, and 8.67 % for Top-A, Top-N, and Bottom-BI,

respectively. Both R_{sh} mapping images of Top-A and Top-N are not uniform. On the other hand, the R_{sh} mapping image of Bottom-BI is very uniform, indicating that BI molecules were uniformly adsorbed on the graphene surface.

After dual-side doping process, the variation decreases to 9.28 % for Dual-A, and 6.42 % for Dual-N, showing a uniform blue color. Consequently, the bottom-side doping played a vital role for the uniform doping, and the dual-side doping allowed the graphene to have a low R_{sh} along with uniform charge distribution.

Atomic force microscopy (AFM) morphological images of the PG, Dual-A, and Dual-N are shown in Fig. 3**(d-f)**. The root-mean-square (RMS, R_q) roughness of PG is 1.25 nm, coming from wrinkle, PMMA residues, and damages during the transferred process [24]. The RMS of Dual-A (4.30 nm) is much higher due to the aggregation of reduced Au cations than that of Dual-N (0.54 nm), infering that the Dual-N could lessen the electrical leakage.

3.4. Stability of dual-side doped graphene films

R_{sh} changes (R/R_0) were measured to compare the stability among the samples. Chemical stability was tested by dipping the Dual-A and Dual-N samples into the acid (AA; acetic acid, K_a: $\sim 1.8 \times 10^{-5}$), strong base (SH; sodium hydroxide, $K_b > 1$), or weak base (AH; ammonium hydroxide, K_b: $\sim 1.8 \times 10^{-5}$). R_0 is the initial R_{sh}, R is the R_{sh} after acid/base treatment. The R_{sh} of Dual-A was significantly increased, but that of Dual-N was maintained regardless the types of acid/base (Fig. 4**a**).

The changes of XPS spectra of Au 4f, Cl 2p, F 1 s, and S 2p are shown **in** Fig. 4**(c)-(f)** before and after AA treatment. In the case of Dual-A, the peaks of Cl 2p (~198 eV, ~200 eV) were completely diminished and the peaks of Au^{3+} cations (~87 eV, ~91 eV) were also reduced, suggesting that the $AuCl_3$ dopant was unstable to the chemical treatments, leading to the increased R_{sh}. In the case of Dual-N, no obvious degredation of XPS peaks (F 1 s and S 2p) was observed with a little peak shift to a higher energy. This implies that the Nafion had a high stability against the acid/base solution, leading to the stable R_{sh}. XPS spectral changes after other acids/bases treatment are included in **Fig. S9**. Regardless of the types of acid/base, XPS spectral change had a similar tendency between the two samples.

Moreover, polar aprotic (isopropyl alcohol, dimethyl sulfoxide) and non-polar (toluene) solvents were spin-casted on the Dual-A and Dual-N to evaluate chemical resistance against those. The R_{sh} of Dual-A was increased; however, the R_{sh} of Dual-N was negligibly changed (Fig. 4**b**). These results also demonstrate that the Dual-N was stable under harsh chemical environments. The reason for the outstanding stability can be expected owing to the fluorocarbon backbone of Nafion, which reduces the surface energy of Dual-N and thus repulses the molecules of acids/bases and solvents [41,42].

R_{sh} changes were also measured after annealing at different temperatures (Fig. 4**(g)**) and then the film stability was analyzed by using XPS (Fig. 4**(h) and Fig. S10**). The R_{sh} of Dual-A was slightly increased after 100 °C annealing, but de-doping of Dual-A was occurred at 200 °C to increase the R_{sh} by 700 %. With increasing the annealing temperature, the proportion of Cl atom decreased from 17.24 % (as-doped) to 11.94 % (100 °C), 3.14 % (200 °C) and the proportion of Au^{3+} ion also decreased from 3.63 % (as-doped) to 3.03 % (100 °C), 0.99 % (200 °C). Because the Cl adsorption was favorably occurred under appropriate moisture condition [43,44], the negatively charged Cl ions on the graphene surface were desorbed at such a high annealing temperature, rendering the reduction of electrostatically balanced Au^{3+} ions into Au^0 clusters. As a consequence, the dopants of Dual-A were not stable to increase the R_{sh} at a high temperature.

In comparison, the R_{sh} of Dual-N was even decreased after 200 °C annealing **(**Fig. 4**(g))**. It is reported that thermal annealing caused the arrangement of sulfonic acid groups of Nafion towards the underlying graphene [41,42]. The electron-withdrawing of sulfonic acid groups near the graphene resulted in more *p*-doped graphene, inducing the slight reduction of R_{sh}. The dopant survived after thermal treatment in the case of Dual-N; the proportion of F 1 s was slightly reduced from 61.23 % (as-doped) to 53 % (200 °C), and that of S 2p was reduced from 1.92 % (as-doped) to 1.78 % (100 °C), 1.76 % (200 °C). To sum up, the Dual-N has superior properties in terms of thermal/chemical stability compared to the Dual-A.

4. Conclusion

We demonstrated dual-side doping of graphene for achieving high FoM (σ_{DC}/σ_{op}) values, uniform doping, and high stability against thermal/chemical environments. The electrical and optical properties, and the thermal/chemical stability were compared with two different top-side dopants ($AuCl_3$ and Nafion). Both Dual-A ($AuCl_3$ top dopant and BI bottom dopant) and Dual-N (Nafion top dopant and BI bottom dopant) demonstrated a strong *p*-doping effect as well as uniform doping with uniformity variation less than 10 %. The best FoM value of 62.38 was achieved with the Dual-N at 50 mM Nafion concentration. In addition, the Dual-N had a strong stability against harsh chemical conditions and elevated temperature, providing significant advancements in graphene electrodes for practical (flexible and transparent) applications.

CRediT authorship contribution statement

Min Ji Im: Conceptualization, Investigation, Visualization. **Seok-Ki Hyeong:** Methodology, Data curation. **Jae-Hyun Lee:** Methodology, Data curation. **Gun Young Jung:** Funding acquisition, Supervision, Writing - review & editing. **Sukang Bae:** Conceptualization, Investigation, Funding acquisition, Supervision, Writing – review & editing. **Tae-Wook Kim:** Formal analysis, Methodology, Data curation. **Seoung-Ki Lee:** Formal analysis, Methodology, Data curation.

Declaration of Competing Interest

The authors declare that they have no known competing financial interests or personal relationships that could have appeared to influence the work reported in this paper.

Acknowledgements

G.Y. Jung was partially supported by the National Research Foundation of Korea (NRF) grant funded by the Korea government (MSIT) [NRF-2022R1A2B5B01002038]. S. Bae was financially supported by the Korea Institute of Science and Technology (KIST) Institutional Program, the Ministry of Trade, Industry & Energy of Korea (20011317), and the National Research Council of Science & Technology (NST) grant [CRC-20-01-NFRI].

Appendix A. Supplementary material

Supplementary data to this article can be found online at https://doi.org/10.1016/j.apsusc.2022.154569.

References

[1] Y. Lee, S. Bae, H. Jang, S. Jang, S.E. Zhu, S.H. Sim, Y.I. Song, B.H. Hong, J.H. Ahn, Wafer-scale synthesis and transfer of graphene films, Nano Lett. 10 (2) (2010) 490–493, https://doi.org/10.1021/nl903272n.

[2] G. Jo, M. Choe, S. Lee, W. Park, Y.H. Kahng, T. Lee, The application of graphene as electrodes in electrical and optical devices, Nanotechnology 23 (11) (2012), 112001, https://doi.org/10.1088/0957-4484/23/11/112001.

[3] A.K. Geim, Graphene status and prospects, Science 324 (19) (2009) 1530–1534, https://doi.org/10.1126/science.1158877.

[4] S.-H. Bae, X. Zhou, S. Kim, Y.S. Lee, S.S. Cruz, Y. Kim, J.B. Hannon, Y. Tang, D. D. Sadna, F.M. Ross, H. Park, J. Kim, Unveiling the carrier transport mechanism in epitaxial graphene for forming wafer-scale, single-domain graphene, PNAS 114 (16) (2017) 4082–4086, https://doi.org/10.1073/pnas.1620176114.

[5] J.H. Lee, E.K. Lee, W.-J. Joo, Y. Jang, B.-S. Kim, J.Y. Lim, S.-H. Choi, S.J. Ahn, J. R. Ahn, M.-H. Park, C.-W. Yang, B.L. Choi, S.-W. Hwang, D. Whang, Wafer-scale growth of single-crystal monolayer graphene on reusable hydrogen-terminated germanium, Science 344 (6181) (2014) 286–289, https://doi.org/10.1126/Science.1252268.

[6] J.D. Wood, S.W. Schmucker, A.S. Lyons, E. Pop, J.W. Lyding, Effects of polycrystalline Cu substrate on graphene growth by chemical vapor deposition, Nano Lett. 11 (11) (2011) 4547–4554, https://doi.org/10.1021/nl201566c.

[7] D. Lee, G.D. Kwon, J.H. Kim, E. Moyen, Y.H. Lee, S. Baik, D. Pribat, Significant enhancement of the electrical transport of graphene films by controlling the surfac roughness of Cu foils before and during chemical bapor deposition, Nanoscale 6 (2014) 12943–12951, https://doi.org/10.1039/C4NR03633F.

[8] S. Bae, H. Kim, Y. Lee, X. Xu, J.S. Park, Y. Zheng, J. Balakrishnan, T. Lei, H.R. Kim, Y.I. Song, Y.J. Kim, K.S. Kim, B. Ozyilmaz, J.H. Ahn, B.H. Hong, S. Iijima, Roll-to-roll production of 30-inch graphene films for transparent electrodes, Nat. Nanotechnol. 5 (8) (2010) 574–578, https://doi.org/10.1038/nnano.2010.132.

[9] T.-H. Han, Y. Lee, M.-R. Choi, S.-H. Woo, S.-H. Bae, B.H. Hong, J.-H. Ahn, T.-W. Lee, Extremely efficient flexible organic light-emitting diodes with modified graphene anode, Nat. Photonics 6 (2) (2012) 105–110, https://doi.org/10.1038/nphoton.2011.318.

[10] K.C. Kwon, K.S. Choi, S.Y. Kim, Increased work function in few-layer graphene sheets via metal chloride doping, Adv. Func. Mater. 22 (22) (2012) 4724–4731, https://doi.org/10.1002/adfm.201200997.

[11] T.L. Wu, C.H. Yeh, W.T. Hsiao, P.Y. Huang, M.J. Huang, Y.H. Chiang, C.H. Cheng, R.S. Liu, P.W. Chiu, High-performance organic light-emitting diode with substitutionally boron-doped graphene anode, ACS Appl. Mater. Interfaces. 9 (17) (2017) 14998–15004, https://doi.org/10.1021/acsami.7b03597.

[12] M. Kim, K.-J. Kim, S.J. Lee, H.-M. Kim, S.-Y. Cho, M.-S. Kim, S.-H. Kim, K.-B. Kim, Highly stable and effective doping of graphene by selective atomic layer deposition of ruthenium, ACS Appl. Mater. Interfaces. 9 (2017) 701–709, https://doi.org/10.1021/acsami.6b12622.

[13] M.H. Kang, G. Qiu, B. Chen, A. Jouvray, K.B.K. Teo, C. Cepek, L. Wu, J. Kim, W. I. Milne, M.T. Cole, Transport in polymer-supported chemically-doped CVD graphSene, J. Mater. Chem. C. 5 (2017) 9886–9897.

[14] E. Shi, H. Li, L. Yang, L. Zhang, Z. Li, P. Li, Y. Shang, S. Wu, X. Li, J. Wei, K. Wang, H. Zhu, D. Wu, Y. Fang, A. Cao, Colloidal antireflection coating improves graphene-silicon solar cells, Nano Lett. 13 (4) (2013) 1776–1781, https://doi.org/10.1021/nl400353f.

[15] Y. Song, X. Li, C. Mackin, X. Zhang, W. Fang, T. Palacios, H. Zhu, J. Kong, Role of interfacial oxide in high-efficiency graphene-silicon Schottky barrier solar cells, Nano Lett. 15 (3) (2015) 2104–2110, https://doi.org/10.1021/nl505011f.

[16] G. Ahn, S. Ryu, Reversible sulfuric acid doping of graphene probed by in-situ multi-wavelength Raman spectroscopy, Carbon. 138 (2018) 257–263, https://doi.org/10.1016/j.carbon.2018.05.065.

[17] T. Cui, R. Lv, Z.-H. Huang, S. Chen, Z. Zhang, X. Gan, Y. Jia, X. Li, K. Wang, D. Wu, F. Kang, Enhanced efficiency of graphene/silicon heterojunction solar cells by molecular doping, J. Mater. Chem. A. 1 (18) (2013) 5736–5740, https://doi.org/10.1039/c3ta01634j.

[18] D.H. Shin, J.M. Kim, C.W. Jang, J.H. Kim, S. Kim, S.-H. Choi, Effect of layer number and metal-chloride dopant on multiple layers of graphene/porous Si solar cells, J. Appl. Phys. 123 (12) (2018) 121301–121307, https://doi.org/10.1063/1.5013169.

[19] K.K. Kim, A. Reina, Y. Shi, H. Park, L.J. Li, Y.H. Lee, J. Kong, Enhancing the conductivity of transparent graphene films via doping, Nanotechnology 21 (28) (2010), 285205, https://doi.org/10.1088/0957-4484/21/28/285205.

[20] C. Park, D. Yoo, S. Im, S. Kim, W. Cho, J. Ryu, J.H. Kim, Large-scalable RTCVD Graphene/PEDOT:PSS hybrid conductive film for application in transparent and flexible thermoelectric nanogenerators, RSC Adv. 7 (41) (2017) 25237–25243, https://doi.org/10.1039/c7ra02980b.

[21] Y. Qian, I. Jeon, Y.L. Ho, C. Lee, S. Jeong, C. Delacou, S. Seo, A. Anisimov, E. I. Kaupinnen, Y. Matsuo, Y. Kang, H.S. Lee, D. Kim, J.J. Delaunay, S. Maruyama, Multifunctional effect of *p*-Doping, antireflection, and encapsulation by polymeric acid for High efficiency and stable carbon nanotube-based silicon solar cells, Adv. Energy Mater. 10 (1) (2020) 1902389, https://doi.org/10.1002/aenm.201902389.

[22] J.H. Heo, D.H. Shin, D.H. Song, D.H. Kim, S.J. Lee, S.H. Im, Super-flexible bis (trifluoromethanesulfonyl)-amide doped graphene transparent conductive electrodes for photo-stable perovskite solar cells, J. Mater. Chem. A. 6 (18) (2018) 8251–8258, https://doi.org/10.1039/c8ta02672f.

[23] A.K. Singh, V. Chaudhary, A.K. Singh, S.R.P. Sinha, Investigation of electronic properties of chemical vapor deposition grown single layer graphene via doping of thin transparent conductive films, RSC Adv. 11 (5) (2021) 3096–3103, https://doi.org/10.1039/d0ra10057a.

[24] Y. Yao, S.A. Peng, X.N. Huang, D.Y. Zhang, J.Y. Shi, Z. Jin, A uniform stable P-type graphene doping method with a gold etching process, Nanotechnology 30 (40) (2019), 405205, https://doi.org/10.1088/1361-6528/ab2e33.

[25] K.C. Kwon, B.J. Kim, J.-L. Lee, S.Y. Kim, Role of ionic chlorine in the thermal degradation of metal chloride-doped graphene sheets, J. Mater. Chem. C. 1 (2) (2013) 253–259, https://doi.org/10.1039/c2tc00008c.

[26] K.C. Kwon, S.Y. Kim, Extended thermal stability in metal-chloride doped graphene using graphene overlayers, Chem. Eng. J. 244 (2014) 355–363, https://doi.org/10.1016/j.cej.2014.01.100.

[27] J.S. Kim, B.J. Kim, Y.J. Choi, M.H. Lee, M.S. Kang, J.H. Cho, An organic vertical field-effect transistor with underside-doped graphene electrodes, Adv. Mater. 28 (24) (2016) 4803–4810, https://doi.org/10.1002/adma.201505378.

[28] K. Jo, S.-M. Kim, S.-M. Lee, J.-H. Kim, H.-J. Lee, K.S. Kim, Y.D. Kwon, K.-S. Kim, One-step etching, doping, and adhesion-control process for graphene electrodes, Carbon. 82 (2015) 168–175, https://doi.org/10.1016/j.carbon.2014.10.059.

[29] Y. Kim, J. Park, J. Kang, J.M. Yoo, K. Choi, E.S. Kim, J.B. Choi, C. Hwang, K. S. Novoselov, B.H. Hong, A highly conducting graphene film with dual-side molecular *n*-doping, Nanoscale 6 (16) (2014) 9545–9549, https://doi.org/10.1039/c4nr00479e.

[30] D. Xu, J. He, X. Yu, D. Gao, L. Ma, X. Mu, M. Zhong, Y. Xu, J. Ye, M. Xu, D. Yang, Illumination-induced hole doping for performance improvement of graphene/n-silicon solar cells with P3HT interlayer, Adv. Electron. Mater. 1600516 (3) (2017) 1–9, https://doi.org/10.1002/aelm.201600516.

[31] S.J. Kim, J. Ryu, S. Son, J.M. Yoo, J.B. Park, D. Won, E.-K. Lee, S.-P. Cho, S. Bae, S. Cho, B.H. Hong, Simultaneous etching and doping by Cu-stabilizing agent for high-performance graphene-based transparent electrodes, Chem. Mater. 26 (7) (2014) 2332–2336, https://doi.org/10.1021/cm500335y.

[32] Z.H. Ni, H.M. Wang, Z.Q. Luo, Y.Y. Wang, T. Yu, Y.H. Wu, Z.X. Shen, The effect of vacuum annealing on graphene, J. Raman Spectrosc. 41 (5) (2010) 479–483, https://doi.org/10.1002/jrs.2485.

[33] P.K. Nayak, Pulsed-grown graphene for flexible transparent conductors, Nanoscale Adv. 1 (3) (2019) 1215–1223, https://doi.org/10.1039/c8na00181b.

[34] G. Robert Bigras, X. Glad, P. Vinchon, R. Martel, L. Stafford, Selective nitrogen doping of graphene due to preferential healing of plasma-generated defects near grain oundaries, npj 2D Mater. and Appl. (1) (2020) 42, https://doi.org/10.1038/41699-020-00176.

[35] S. Tongay, K. Berke, M. Lemaitre, Z. Nasrollahi, D.B. Tanner, A.F. Hebard, B. R. Appleton, Stable hole doping of graphene for low electrical resistance and high optical transparency, Nanotechnology 22 (42) (2011) 425701.

[36] J.-Y. Syu, Y.-M. Chen, K.-X. Xu, S.-M. He, W.-C. Hung, C.-L. Chang, C.-Y. Su, Wide-range work-function tuning of active graphene transparent electrodes via hole doping, RSC Adv 6 (2016) 32746–32756, https://doi.org/10.1039/c6ra04449b.

[37] A. Das, S. Pisana, B. Chakraborty, S. Piscanec, S.K. Saha, U.V. Waghmare, K. S. Novoselov, H.R. Krishnamurthy, A.K. Geim, A.C. Ferrari, A.K. Sood, Monitoring dopants by Raman scattering in an electrochemically top-gated graphene transistor, Nat. Nanotechnol. 3 (4) (2008) 210–1205, https://doi.org/10.1038/nnano.2008.67.

[38] B.-J. Lee. C.-W. Huang, H.-Y Lin, C.-H. Huang, F.-Y. Shih, W.-H. Wang, C.-Y. Liu1, H.-C. Chui, Surface-enhanced raman scattering of suspended monolayer graphene, Nano Express. 8 (1) (2013) 480, https://doi.org/https://doi.org/10.1186/1556-276X-8-480.

[39] L.P. Ma, Z. Wu, L. Yin, D. Zhang, S. Dong, Q. Zhang, M.L. Chen, W. Ma, Z. Zhang, J. Du, D.M. Sun, K. Liu, X. Duan, D. Ma, H.M. Cheng, W. Ren, Pushing the conductance and transparency limit of monolayer graphene electrodes for flexible organic light-emitting diodes, Proc. Natl. Acad. Sci. USA 117 (42) (2020) 25991–25998, https://doi.org/10.1073/pnas.1922521117.

[40] S. Da, J.N. Coleman, Are there fundamental limitations on the sheet resistance atransmittance of thin graphene films, ACS Nano. 4 (5) (2010) 2713–2720, https://doi.org/10.1021/nn100343f.

[41] S-.J. Kwon, T-.H. Han, T-.Y. Ko, N-. Li, T. Kim, D.J. Kim, S-.H. Bae, Y. Yang, B. H. Hong, K.S. Kim, S. Ryu, T-.W. Lee, Extremely stable graphene electrodes doped with macromolecular acid, Nat Comm 50 (9) (2018) 2037, https://doi.org/10.1038/s41467-018-04385-4.

[42] D.K. Paul, K. Karan, Effect of thermal treatment on the properties of ultra-thin nafion film, ECS Trans. 50 (9) (2018) 951–959, https://doi.org/10.1038/s41467-018-04385-4.

[43] K.C. Kwon, B.J. Kim, J.-L. Lee, S.Y. Kim, Effect of anions in Au complexes on doping and degradation of graphene, J. Mater. Chem. C. 1 (13) (2013) 2463–2469, https://doi.org/10.1039/c3tc00046j.

[44] K.K. Kim, S.M. Kim, Y.W. Jo, M.H. Park, S.J. Chae, D.L. Duong, C.W. Yang, J. Kong, Y.H. Lee, Role of Anions in the $AuCl_3$-Doping of Carbon Nanotubes, ACS Nano 5 (2) (2011) 1236–1242, https://doi.org/10.1021/nn1028532.